

ConDA: Unsupervised Domain Adaptation for LiDAR Segmentation via Regularized Domain Concatenation

Lingdong Kong^{1,2,*} Niamul Quader¹ Venice Erin Liong¹

¹Motional, ²Nanyang Technological University

lingdong001@e.ntu.edu.sg, niamul.quader@motional.com, venice.liong@motional.com

Abstract

Transferring knowledge learned from the labeled source domain to the raw target domain for unsupervised domain adaptation (UDA) is essential to the scalable deployment of an autonomous driving system. State-of-the-art approaches in UDA often employ a key concept: utilize joint supervision signals from both the source domain (with ground-truth) and the target domain (with pseudo-labels) for self-training. In this work, we improve and extend on this aspect. We present ConDA, a concatenation-based domain adaptation framework for LiDAR semantic segmentation that: (1) constructs an intermediate domain consisting of fine-grained interchange signals from both source and target domains without destabilizing the semantic coherency of objects and background around the ego-vehicle; and (2) utilizes the intermediate domain for self-training. Additionally, to improve both the network training on the source domain and self-training on the intermediate domain, we propose an anti-aliasing regularizer and an entropy aggregator to reduce the detrimental effects of aliasing artifacts and noisy target predictions. Through extensive experiments, we demonstrate that ConDA is significantly more effective in mitigating the domain gap compared to prior arts.

1. Introduction

Large sets of annotated data are always desirable since they often lead to robust and deployable models. However, annotating semantic labels for 3D data like LiDAR point clouds [29] in autonomous driving [3, 5, 7, 14, 19, 24, 53] is extremely expensive and labor-intensive [18, 71], and thus it is practically prohibitive to label every sample collected [65]. The contradiction between desire and fact motivates our community to explore unsupervised domain adaptation (UDA) for knowledge transfer [42].

UDA aims to tackle situations where a model is trained with labeled data from a source domain $\mathcal{D} = s$ and unlabeled data from a different but related target domain $\mathcal{D} = t$,

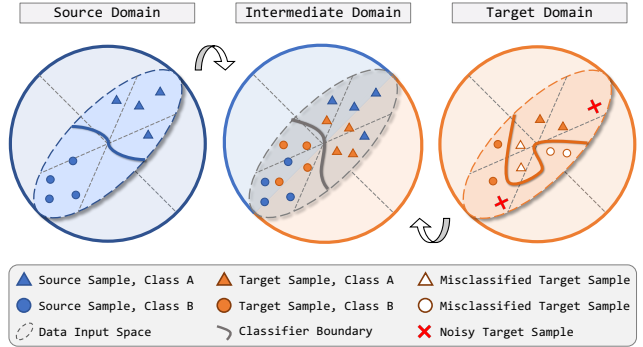


Figure 1. Conceptual illustration of regularized domain concatenation. Proper classifier boundary can be delineated under supervised learning fashion for the labeled source domain (left). The unlabeled target domain (right) suffers from discrepancies, often resulting in massive false predictions if the source model is directly used on target. We propose to explicitly bridge the source and target by an intermediate domain (middle), where fine-grained interchanges from both domains are introduced. This is achieved by concatenating the range-view projection stripes of the source and target LiDAR point clouds and regularizing the target entropy.

beled data from a different but related target domain $\mathcal{D} = t$, with the goal of enabling the model to perform well during target test time. This is broadly achieved by learning jointly from both the source and target domains [54], where the learning mechanism in prior arts mainly follows two lines: (1) implicit learning domain-invariant features with domain discriminators via adversarial learning [16, 17, 20], and (2) self-training with joint supervision signals from both the source domain (with ground-truth) and the target domain (with pseudo-labels selected by confidence thresholding) [28, 77]. Recent works have shown that approaches based on self-training often yield more robust models while being less expensive computationally [2, 79]. These approaches, however, learn separately from source and target batches, and thus lack of learning fine-grained interactions of objects and background in-between domains. Implementing an intermediate domain (cf. Fig. 1) that can facilitate such interactions is intuitive. The ground-truth signals from the source domain can construct a “shortcut” for correcting

*Work done during his internship at Motional.

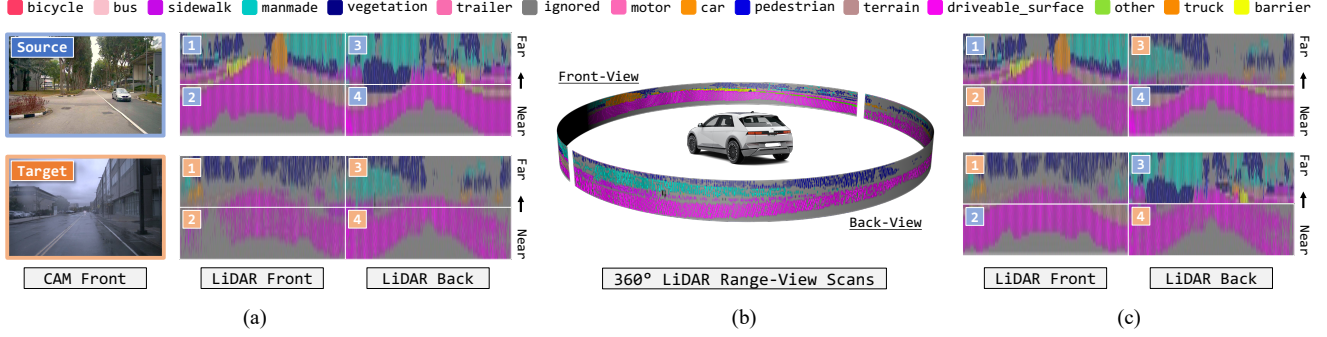


Figure 2. Illustrative examples for domain concatenation. (a) Visual RGB and LiDAR range-view (RV) projections of the source (ground-truth) and target (pseudo-labels) domains. Images adopted from nuScenes [5]. (b) Cylindrical representation of LiDAR RV. (c) Concatenated examples. Mixing domains using our ConDA strategy yields semantically realistic intermediate domain samples for self-training.

false target predictions in the local vicinity since feature representations close to each other tend to have the same semantic label [34]. Additionally, the target “pseudo supervisions” – which often contain large amounts of ignored labels – can serve as a strong consistency regularization [15] for the source domain. This guided supervision and regularization may yield a more adaptable and robust feature learning. It is not easy, however, to directly mix domains via interpolation [4, 59, 73] or superposition [11, 72] for semantic segmentation as such techniques can corrupt the semantic coherency of the mixed/intermediate domain [15].

In this work, we propose a concatenation-based domain adaptation (ConDA) approach for UDA in LiDAR segmentation which enables the interactions of fine-grained semantic information in-between the source and target domains while not destabilizing the semantic coherency. We make the observations that although the overall distributions for the source and target domains are very different, there is a strong likelihood that similar objects and background tend to occupy particular regions in the LiDAR range-view (RV) around the ego-vehicle (*cf.* Fig. 2b). As an example, the bottom-half views of both source and target domains are mostly composed of ‘driveable surface’, whereas the upper-half views tend to contain ‘barrier’, ‘car’, ‘vegetation’, etc. (*cf.* Fig. 2a). We exploit this important correlation to construct the ConDA intermediate domain that selects non-overlapping regions of point clouds from both source and target domains and concatenates them together, while maintaining the relative positions from the ego-vehicle. As shown in Fig. 2c, concatenating different regions (*e.g.*, front-top, front-bottom, back-top, and back-bottom) of RV stripes from different domains can still preserve semantic consistency. We will revisit this formally in Sec. 3.2.

The proposed domain concatenation strategy provides a better solution for model self-training via interchanged supervisions from both the source domain and the target domain. It is worth noting that the quality of the pseudo-labels – and in turn the generalizability of the initial training on the

source domain – becomes essential since erroneous “pseudo supervision” can do evil in self-training. We counter this problem from two perspectives as follows.

First, the generalizability of the model can be considerably improved by removing high-frequency aliasing artifacts [58, 74] with careful placements of low-pass anti-aliasing filters [78]. However, empirically designing such filters is challenging in the context of UDA, since the lack of target domain ground-truth prevents any empirical experiments. To reduce the detrimental effect of high-frequency aliasing artifacts [6, 51] without access to annotations, we propose a built-in regularization mechanism (*cf.* Sec. 3.3) within each convolution block to regularize high-frequency representation learning during training.

Furthermore, as the pseudo-labels are “guessed” by the model trained on the source domain, it is intuitive to leverage the uncertainty [21] of such “guesses” for filtering non-confident selections. Entropy [50] – a measure of choice freedom – has been proved conducive in recent works for estimating prediction uncertainty [63, 76]. Different from prior arts that implicitly minimize entropy in an adversarial way [41, 60], we design an entropy aggregator (*cf.* Sec. 3.4) which explicitly eliminates high entropy target predictions and thus improves the overall quality for the intermediate domain supervisions.

Overall, this work has the following key contributions:

- We propose ConDA, a novel framework for UDA that facilitates fine-grained interactive learning in-between the source and target domains. To the best of our knowledge, we are the first work that explored uni-modal UDA for cross-city LiDAR segmentation, which can serve as a baseline for future research.
- We design two regularization techniques to reduce the detrimental aliasing artifacts and uncertain target predictions during model pre-training and self-training.
- We conduct comprehensive studies on the effects of our technical contributions on two challenging UDA

scenarios in nuScenes [5]. Our methods provide significant performance gains over state-of-the-art UDA approaches.

2. Related Work

UDA on Visual RGB. Adversarial training [16, 17] and self-training [28, 77] dominate almost all kinds of 2D scene adaptation scenarios [9, 10, 39, 46, 47, 49, 70]. Methods based on adversarial training adopt domain discriminators [20, 44] to implicitly search for domain-invariant features via distance measurements at different levels, *i.e.*, input-level [23, 36, 55, 68, 69], feature-level [13, 33, 66], and output-level [57, 60, 61]. However, such methods suffer from high computational costs and tend to be sensitive to hyperparameters and target domain changes [25, 35]. Self-training, on the other hand, offers a lighter option by joint learning from both source and target domain supervisions [64], where the latter can be generated via confidence thresholding [30, 79, 80]. More recent works even combine self-training with style transfer [8, 27, 62] and adversarial pre-training [12, 37, 41, 76]. Evidence shows that these methods – albeit powerful in 2D – become less effective in 3D [25, 43], which motivates us to design new methods w.r.t. the characteristics of the LiDAR data.

UDA on LiDAR Point Clouds. Adaptations are more challenging in the 3D world as point clouds are sparse, unstructured, and have limited visual cues compared to images [56]. Alonso *et al.* [1] proposed to use shifting to align domain appearances. ePointDA [75] learns a dropout noise rendering from real-world data to match synthetic data. LiDARNet [26] employs two discriminators that jointly adapt for segmentation and boundary prediction. xMUDA [25] and DsCML [43] employ self-training alongside cross-modality learning for cross-location adaptations. However, the assumption of having access to synchronized RGB and LiDAR data in both source and target domains is not always practical, which limits such methods. Our framework does not require data from multiple modalities thus maintaining both simplicity and efficiency for practitioners.

Domain Mixed Inputs. Mixing-based strategies [11, 72, 73] have been widely adopted in fully- [48, 67] and semi- [4, 40, 59] supervised learning tasks, but very few touched UDA. SimROD [45] proposed to create 2x2 collages with two source images (labels) and two target images (pseudo-labels) for robust object detection. DACS [55] cuts source objects out and pastes them onto the target images, alongside mixing corresponding source labels and target pseudo-labels. While the former [45] can corrupt the semantic consistency, the latter [55] requires extra costs for the “copy-paste” operation and lacks mixing background and target objects. Our ConDA provides more fine-grained interactions in-between domains and the concatenations are performed on the fly in self-training with almost zero cost.

Regularization. Anti-aliasing filters are popularly applied to reduce the aliasing artifacts in networks [58, 74, 78]. Such regularizers, however, have not been used in UDA. We conjecture that this is because the empirical observations required in filter design become impractical on the annotation-void target domain. In this work, we adopt a learning-based approach as an alternative to regularize aliasing artifacts during network training. Another type of regularization is uncertainty estimation, which has been proved useful in semi-supervised learning [21]. For UDA, [63] proposed to resample more source data that contain high entropy classes in target predictions. IntraDA [41] uses a discriminator to close the gap between the low-entropy and high-entropy samples. We design an entropy aggregator to disable the usage of non-confident pseudo-labels during domain adaptation, which directly reduces the uncertainty for the intermediate domain supervisions.

3. Technical Approach

The proposed ConDA consists of three major components as shown in Fig. 3. We first document the generic layout for LiDAR segmentation in range-view (RV) as preliminaries (Sec. 3.1). The domain concatenation strategy leverages the advantage of RV representations for constructing the intermediate domain (Sec. 3.2). To further improve the network training on the source domain and self-training on the intermediate domain, we design an anti-aliasing regularizer (Sec. 3.3) and an entropy aggregator (Sec. 3.4) to reduce the aliasing artifacts and noisy target predictions. The overall training procedure is summarized in Algo. 1.

3.1. Preliminaries

RV Projection. Let \mathcal{A} denote LiDAR point clouds. We project each point $\mathbf{o} = (x, y, z)$ on the 360° scans in \mathcal{A} via a mapping $\Pi : \mathbb{R}^3 \mapsto \mathbb{R}^2$ to a cylindrical RV image $\mathbf{a} \in \mathbb{R}^{(6, h, w)}$ with height h and width w [38]. To cover more points, h is set based on the number of rings for the LiDAR sensors, and w is determined by the horizontal angular resolution. Each pixel in \mathbf{a} is composed of the point coordinates (x, y, z) , intensity, range $\|\mathbf{o}\|_2$, and a binary mask (indicates whether or not a point occupies a pixel). The closest point to the sensor is chosen to represent the pixel if multiple points are projected to the same pixel location. Samples from the source domain $\mathcal{D} = s$ and target domain $\mathcal{D} = t$ are processed by the same operations. Note that the RV projections preserve the range information and the spatial correspondence for the LiDAR scans, *e.g.*, the near-front and far-front points are projected onto the left-bottom and left-top of the RV images, respectively, which is a unique feature of the LiDAR representations.

Segmentation Network. To extract features from \mathbf{a} efficiently, we design a fully-convolutional network \mathcal{G} with strided convolutions [31] and skip-connections [22] as our

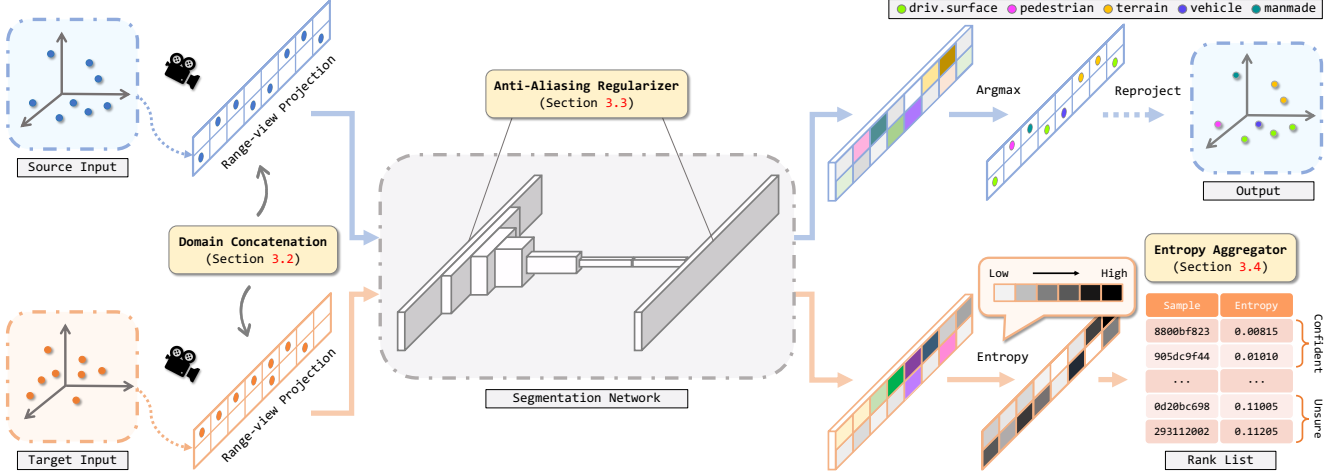


Figure 3. Overview of our concatenation-based domain adaptation (ConDA) framework. After preprocessing (Sec. 3.1), sample stripes from the source domain and target domain are mixed via RV concatenation (Sec. 3.2). The concatenated inputs are fed into the segmentation network for feature extraction and prediction. We include anti-aliasing regularizers inside convolution operations (Sec. 3.3) to suppress the learning of high-frequency aliasing artifacts. The segmented RV cells are then projected back to the point clouds. Here the target prediction part is omitted for simplicity. To mitigate the impediment caused by erroneous target predictions, we design an entropy aggregator (Sec. 3.4) which splits target samples into a confident set and an unsure set and disables the usage of samples from the latter set.

backbone. \mathcal{G} consists of seven stages (cf. Fig. 3). Since h is much smaller than w , we only downsample the height at later stages. The segmentation head combines the upsampled output features from the last four stages for multi-scale feature aggregations. More details on our segmentation network are in Appendix.

3.2. Domain Concatenation

In the context of UDA for LiDAR segmentation, we denote samples from the labeled source domain and unlabeled target domain as $\mathcal{A}_s = \{\mathbf{a}_s^i, \mathbf{y}_s^i\}_{i=1}^M$ and $\mathcal{A}_t = \{\mathbf{a}_t^j\}_{j=1}^N$, where M and N are the total number of source and target samples. For segmentation with C classes, the network \mathcal{G} can be optimized in a supervised way with source samples by minimizing the cross-entropy loss as follows:

$$\min_{\mathbf{w}} \mathcal{L}_s = -\frac{1}{|M|} \sum_{\mathbf{a}_s \in M} \sum_{c=1}^C \mathbf{y}_s^{(c)} \log p(c|\mathbf{a}_s, \mathbf{w}), \quad (1)$$

where \mathbf{w} denotes the weights of \mathcal{G} ; $p(\cdot)$ is the probability of class c in the softmax output. Due to the lack of ground-truth in the target domain, we consider the target labels as hidden variables [28] and select the most confident target predictions on the existing model as one-hot “pseudo-labels” $\hat{\mathbf{y}}_t$. The learning objective for the target domain is:

$$\begin{aligned} \min_{\mathbf{w}} \mathcal{L}_t &= -\frac{1}{|N|} \sum_{\mathbf{a}_t \in N} \sum_{c=1}^C \hat{\mathbf{y}}_t^{(c)} \log p(c|\mathbf{a}_t, \mathbf{w}), \\ \text{s.t. } \hat{\mathbf{y}}_t &= \begin{cases} \arg \max_c p(c|\mathbf{a}_t, \mathbf{w}), & \text{if } \max(p(c|\mathbf{a}_t, \mathbf{w})) \geq \theta \\ \text{ignored}, & \text{otherwise} \end{cases} \end{aligned} \quad (2)$$

where θ is a threshold for filtering non-confident pseudo-labels. Similar to [79, 80], we set a proportion parameter k to determine the class-wise thresholds θ_c for each class c to balance the class distributions.

Now given a source batch $\{\mathbf{a}_s, \mathbf{y}_s\}$ and a target batch $\{\mathbf{a}_t, \hat{\mathbf{y}}_t\}$, our intermediate domain construction mechanism $\mathcal{M}(\cdot)$ follows three steps. First, define a template for the total number of segregation regions along the near-far dimension (m) in the RV projections and around the ego-vehicle (n). Fig. 2a shows an example of a domain concatenation with $m = 2$ and $n = 2$, having front-near, front-far, back-near, and back-far regions, respectively. Second, slice regions based on the above template for every sample in both batches. This gives $((b_s + b_t) \times m \times n)$ sliced stripes, where b_s and b_t are the batch sizes. Third, concatenate the stripes while keeping their spatial locations consistent, resulting in $(b_s + b_t)$ intermediate domain samples \mathbf{a}_π . Their labels \mathbf{y}_π can be obtained via the same arrangement of the original labels and pseudo-labels. The segmentation loss \mathcal{L}_π for this intermediate domain can be computed using the mixed batch $\{\mathbf{a}_\pi, \mathbf{y}_\pi\}$ in a way similar to Eq. 1. The overall objective for self-training is to minimize the following:

$$\mathcal{L} = \mathcal{L}_s(\mathbf{w}, \mathbf{y}_s) + \sigma \cdot \mathcal{L}_\pi(\mathbf{w}, \mathbf{y}_\pi), \quad (3)$$

where σ is a coefficient that controls the probability of accessing the intermediate domain.

As shown in Fig. 2c, this simple concatenation approach mixes objects and background from both domains, while still preserving the overall consistency. This stability in semantic coherence comes from the priors that the LiDAR point clouds are unstructured and extremely sparse even af-

ter RV projections. Take the popularly adopted nuScenes dataset [5] as an example. We find that on average 59.93% of RV cells are empty, which could downplay the negative impact of region rearrangement since the degree of continuity is low. Besides, the spatially corresponding regions in RV tend to contain similar objects and background, regardless of the domain shift. A typical example is the ‘driveable surface’ class, which occupies more than 56% of cells in the bottom-half RV projections for both cities (correspond to two domains) in nuScenes [5]. We provide more concrete evidence in the Appendix to support our findings.

3.3. Anti-Aliasing Regularizer

Motivated by the recent findings that removing aliasing artifacts in the convolutional networks can improve generalizability [58], we formulate an anti-aliasing regularizer that is built within each convolution filter in the segmentation network to reduce learning from aliasing artifacts. Our goal is to impose regularization on high-frequency representation learning since they are more susceptible to aliasing artifacts [74, 78]. We achieve this via $\mathbf{f}_{c,r} = \mathbf{f}_r \odot \mathbf{f}_c$, where \mathbf{f}_r denotes our regularizer which consists of learnable parameters having the same size as the convolution filter \mathbf{f}_c ; $\mathbf{f}_{c,r}$ is the regularized filter kernel of each convolution; \odot denotes the Hadamard multiplication. Note that during the earlier stages of training, the network tends to learn low-frequency representations [6, 51] that are robust to aliasing artifacts. This will thereby update \mathbf{f}_r such that it becomes more suited for low-frequency representation learning of $\mathbf{f}_{c,r}$. In later phases of training or UDA self-training, however, the network is more inclined to learn increasingly higher frequency representations [6, 51] and thus becomes more susceptible to aliasing artifacts [58]. The modulation of our \mathbf{f}_r on \mathbf{f}_c regularizes gradient updates corresponding to these high-frequency representations and in particular, regularizes the ones that are considerably different from the earlier network learning. This implicit regularization mechanism at later stages of training makes $\mathbf{f}_{c,r}$ more resistant to high-frequency aliasing artifacts than the plain convolution filter \mathbf{f}_c . Note that, since \mathbf{f}_c and \mathbf{f}_r are both constants during inference, the regularized filter kernel $\mathbf{f}_{c,r}$ only needs to be computed once at the end of training and then can be used at inference without adding any additional computational cost or structural changes to the network.

3.4. Entropy Aggregator

Given the fact that the pseudo-labels generated from the source pre-trained model tend to be noisy [63], we design an entropy aggregator to disable the access of non-confident target predictions and thus improve the overall quality of the intermediate domain supervisions. More formally, given a target sample \mathbf{a}_t , its entropy map \mathcal{E} composed of the normalized pixel-wise entropies can be calculated as follows:

$$\mathcal{E} = \frac{-1}{\log(C)} \sum_{c=1}^C p(c|\mathbf{a}_t, \mathbf{w}) \log p(c|\mathbf{a}_t, \mathbf{w}). \quad (4)$$

The median value \mathbf{e} of \mathcal{E} for each \mathbf{a}_t is used as the global-level indicator of uncertainty, which is more robust than the average value due to the large “noisy” predictions for the empty RV cells. The target set $\mathcal{A}_t = \{\mathbf{a}_t^j\}_{j=1}^N$ is re-organized based on \mathbf{e} and only the pseudo-labels from the top ϖ most confident target samples are included as the supervisions for the intermediate domain (cf. Sec. 3.2).

Integrating our technical contributions, we now present the overall training procedure of ConDA (cf. Algo. 1), which consists of two rounds of self-training that encourage fine-grained interactive learning in-between domains while regularizing anti-aliasing artifacts and non-confident target predictions. As we will show in the next section, these components are complementary to each other and the marriage of them can significantly boost the adaptation performance.

Algorithm 1 ConDA Self-Training Procedure

- 1: **Input:** Source data $\{\mathbf{a}_s, \mathbf{y}_s\}$; target data $\{\mathbf{a}_t\}$; pre-trained backbone weights \mathbf{w}^0 ; parameters ϖ, k, σ
 - 2: **Output:** Self-trained backbone weights \mathbf{w}^{r2}
 - 3: **Round 1:**
 - 4: Calculate $\mathbf{e} = \text{mid}(\mathcal{E})$ for all \mathbf{a}_t with \mathbf{w}^0 via Eq. (4)
 - 5: Sort $\{\mathbf{a}_t\}$ in an ascending order based on \mathbf{e}
 - 6: Keep the top ϖ $\{\mathbf{a}_t\}$ and discard the rest $\rightarrow \{\mathbf{a}_t\}_{\varpi}$
 - 7: Generate pseudo-labels $\{\hat{\mathbf{y}}_t\}_{\varpi}$ with k, \mathbf{w}^0 via Eq. (2)
 - 8: **repeat**
 - 9: $\{\mathbf{a}_\pi^{r1}, \mathbf{y}_\pi^{r1}\} = \mathcal{M}(\{\mathbf{a}_s, \mathbf{y}_s\}, \{\mathbf{a}_t, \hat{\mathbf{y}}_t\}_{\varpi})$ (cf. Sec. 3.2)
 - 10: Calculate loss \mathcal{L} with σ via Eq. (3); update weights
 - 11: **until** convergence $\rightarrow \mathbf{w}^{r1}$
 - 12: **Round 2:**
 - 13: Generate pseudo-labels $\{\hat{\mathbf{y}}_t\}$ with k, \mathbf{w}^{r1} via Eq. (2)
 - 14: **repeat**
 - 15: $\{\mathbf{a}_\pi^{r2}, \mathbf{y}_\pi^{r2}\} = \mathcal{M}(\{\mathbf{a}_s, \mathbf{y}_s\}, \{\mathbf{a}_t, \hat{\mathbf{y}}_t\})$ (cf. Sec. 3.2)
 - 16: Calculate loss \mathcal{L} with σ via Eq. (3); update weights
 - 17: **until** convergence $\rightarrow \mathbf{w}^{r2}$
-

4. Experiments and Analysis

4.1. Settings

Data. We construct two RV-based cross-city UDA scenarios with nuScenes [5] – a large-scale autonomous driving database widely adopted in academia. It consists of 1000 driving scenes with 40k annotated keyframes taken at 2Hz. We split samples based on their geographic locations. This gives 15695 and 12435 training samples and 3090 and 2929 evaluation samples for Boston and Singapore, respectively. All training samples are used as the source/target for adaptations. Different from xMUDA [25] which only assigns se-




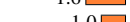
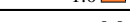
Δ	mIoU	Configuration
-12.0 	34.9	No adaptation (source-only)
-6.2 	40.7	Baseline
-5.0 	41.9	+ Anti-aliasing filters
-1.6 	45.3	+ Domain concatenation
-1.0 	45.9	+ Entropy aggregator (round 1)
0.0	46.9	Full ConDA framework

Table 1. Effectiveness for each component in ConDA. Evaluated on the Boston \rightarrow Singapore adaptation setting.

mantic labels to points inside bounding boxes with 4 object classes and 1 background class, we adopt the *lidarseg*¹ subset in nuScenes which contains 16 classes and fine-grained point-level annotations for LiDAR segmentation.

Implementation Details. The point clouds are transformed into RV images of size 32×1920 as the inputs for the segmentation network (cf. Sec. 3.1). It is first trained from scratch with only source samples for 80 epochs with a batch size of 24 and then fine-tuned under our entropy aggregator-guided self-training procedure (cf. Algo. 1). Both rounds are trained for 20 epochs with the same batch size. We denote results for the supervised learning and direct adaptation as “oracle” and “source-only”. We compare ConDA with eight state-of-the-art methods [30, 41, 57, 60, 61, 79]. We replace their backbones with our segmentation network and keep other configurations in default. The AdamW [32] optimizer is adopted ($\beta_1 = 0.9$, $\beta_2 = 0.999$) with the OneCycle [52] scheduler for pre-training (with learning rate $1e-3$) and the Step scheduler for self-training (with learning rate $1e-4$). For data augmentation, we first employ yaw rotation, jitter, axis flipping, and scaling to the original point clouds and then project augmented points onto RV. For methods based on self-training, we generate their pseudo-labels offline as in [30, 79]. All methods are implemented using PyTorch on NVIDIA Tesla V100 with 16GB RAM.

Evaluation Metrics. We follow the conventional reporting of the intersection-over-union (IoU) scores (%) over each class, the mean IoU (mIoU) and the frequency-weighted IoU (FIoU) scores (%) over all classes in our experiments.

4.2. Ablation Studies

Q1: What is the effect for each component in ConDA?

A1: We adopt the Boston \rightarrow Singapore setting in our ablation studies without the loss of generality. We stratify the three major components in our framework and show their impacts in Tab. 1. Specifically, the anti-aliasing regularizer offers an improvement of 1.2% mIoU over the baseline and surpasses the source-only case by 7.0% mIoU. On top of that, our domain concatenation further improves 3.4% mIoU. Another boost of 1.6% mIoU is achieved under the two-round guidance self-training of our entropy aggregator.

¹<https://www.nuscenes.org/nuscenes#lidarseg>

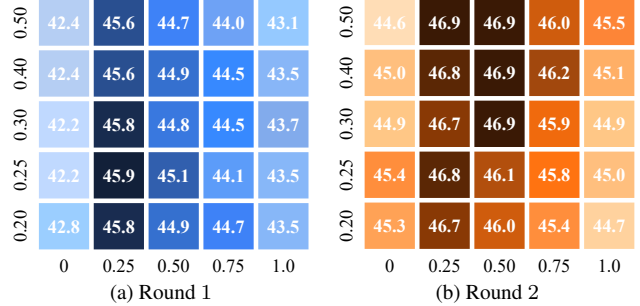


Figure 4. Sensitivity analysis for parameters σ (horizontal axis) and k (vertical axis). Numbers reported are mIoU scores in percentage. The darker the color, the higher the score.

ϖ	0.125	0.25	0.375	0.50	0.625	0.75	0.875	1.0
mIoU	45.0	45.3	45.7	45.9	45.8	45.8	45.4	45.3

Table 2. Sensitivity analysis for the entropy threshold ϖ .

Overall, our framework significantly improves the adaptation results from 34.9% mIoU to 46.9% mIoU, which corresponds to nearly a 34.4% improvement over the source-only and 6.2% mIoU higher than the baseline. We provide additional ablation examples and visualizations in Appendix.

Q2: What are the optimal hyperparameters for ConDA?

A2: We conduct extensive experiments to show the best possible selections for the hyperparameters in our framework. Specifically, the vertical and horizontal axes of Fig. 4 show the impact for the proportion parameter k and the concatenation parameter σ during the two-round self-training while Tab. 2 gives the sensitivity results for the entropy regularization parameter ϖ . We find that lower values for k (e.g. 0.25) in round 1 and relatively higher values (e.g. 0.5) in round 2 tend to give higher mIoU. We conjecture that this relatively conservative choice (or lower value) at round 1 is helpful since pseudo-labels tend to be noisy at this stage. The quality of pseudo-label gets much better in round 2 and including more of them gives a positive impact on the performance. As for σ , we observe that the best possible scores are achieved in between 0.25 and 0.50. Training without ($\sigma = 0$) or with all ($\sigma = 1$) concatenated samples does not perform well. For ϖ (after setting both k and σ as 0.25 without the loss of generality), we find that large ϖ involves more false positives while small ϖ limits the diversity. A compromise value like 0.50 gives the best possible scores.

Q3: What is the best practice for RV concatenation?

A3: Besides the intuitive front-back RV concatenation, we also consider other scenarios as in Fig. 5 and show their results in Tab. 3. As shown, strategies i and l perform the best while j and k offer competitive results. We note that: (1) increasing the granularity of the interactions between source and target tends to improve performance (strategies a to l); (2) increasing the granularity beyond a certain limit

Method	w/o	a	b	c	d	e	f	g	h	i	j	k	l	m	n	o	[45]	[73]	[11]	[72]
mIoU	41.9	43.4	43.5	43.7	44.5	44.6	43.9	44.5	44.6	45.3	45.0	45.2	45.3	44.9	44.6	44.2	33.7	41.1	43.1	42.6

Table 3. Results for different RV concatenation scenarios (cf. Fig. 5) and other mixing techniques.

Method	barr	bicy	bus	car	const	moto	ped	cone	trail	truck	driv	othe	walk	terr	manm	veg	FIoU	mIoU
Oracle	79.5	33.6	87.5	88.9	37.6	75.6	70.5	50.3	0.0	76.2	95.1	53.7	60.2	74.4	83.4	85.5	84.2	65.8
Source-only	29.3	1.3	52.0	71.4	7.2	11.7	42.6	12.2	0.0	30.4	85.9	12.7	32.6	41.0	62.5	65.9	64.3	34.9
AdaptSeg [57]	28.0	7.2	60.9	70.7	7.7	17.4	45.5	14.3	0.0	36.4	88.1	28.4	36.0	43.1	63.0	66.7	66.1	38.3
MinEnt [60]	31.7	4.0	63.7	70.6	5.8	15.9	47.7	13.7	0.1	34.9	87.9	22.4	37.5	41.5	59.9	62.2	64.3	37.5
AdvEnt [60]	28.7	5.9	59.4	76.4	7.2	18.2	50.6	16.7	0.0	32.6	87.0	28.1	36.6	44.0	63.9	67.1	66.3	38.9
DADA [61]	27.4	4.9	60.0	67.7	7.3	15.9	44.4	14.7	0.0	33.9	87.1	21.2	34.9	42.1	62.2	64.9	64.8	36.8
BDL-PL [30]	39.2	0.3	53.0	73.2	6.8	16.0	40.2	8.5	0.0	29.8	88.7	21.3	39.7	48.5	67.1	67.9	68.3	37.5
CBST [79]	39.4	5.3	66.1	75.6	9.3	20.7	47.8	14.9	0.0	34.1	88.4	25.5	38.1	49.9	66.7	68.5	68.6	40.7
AdaptSegPL [57]	29.9	0.3	47.9	64.4	4.9	7.4	28.4	4.6	0.0	24.8	83.1	21.8	38.3	46.5	67.1	68.9	66.0	33.7
IntraDA [41]	28.0	5.6	57.8	76.1	6.2	18.6	47.4	13.8	0.0	32.1	87.3	27.6	37.0	44.4	63.4	66.5	66.2	38.3
ConDA (Ours)	54.1	6.8	67.4	77.2	12.1	38.7	51.8	16.0	0.0	44.0	90.4	38.7	44.0	62.9	70.7	75.0	74.1	46.9

Table 4. Adaptation results for **Boston** \rightarrow **Singapore**. The methods are grouped, from top to bottom, as adversarial training, self-training, both, and ours. All IoU scores are given in percentage. Best score for each class is highlighted in **bold**.

(strategies m , n , and o) can deteriorate performance, which is likely due to the instability in semantic coherence of the objects and background in the concatenated stripes; and (3) fine-grained interactions along the vertical axes (*i.e.*, near to far regions) perform better than interactions along the horizontal axes (*i.e.*, bearing around the ego-vehicle) (cf. strategies i and f in Tab. 3), suggesting that the former likely yields better domain consistency while better maintaining the semantic consistency.

Q4: How is domain concatenation superior to others?

A4: We compare our domain concatenation with four mixing techniques in Tab. 3. SimROD [45] stitched samples from both domains as inputs for adaptation while MixUp [73], CutMix [72], and CutOut [11] are general regularization methods adopted for fully- and semi-supervised learning. While all four methods achieve promising results in their respective RGB-based tasks, they have shown sub-par performance in the RV representation for UDA in LiDAR segmentation. Differently, our approach is able to effectively leverage the spatial context of RV, and combine both the source and target domains into an intermediate domain for fine-grained interactive learning and regularization.

4.3. Comparison to State-of-the-Art

Benchmarking Results. We compare ConDA with eight state-of-the-art methods on the Boston \rightarrow Singapore and Singapore \rightarrow Boston scenarios in Tab. 4 and Tab. 5. In both cases, ConDA substantially outperforms other competitors in terms of mIoU and FIoU. We observe relatively higher adaptation scores for static classes such as ‘driveable surface’ and ‘vegetation’ and lower scores for dynamic classes such as ‘barrier’ and ‘motor’. Notably, in contrast to prior approaches that tend to improve performance on relatively easier classes (*i.e.*, classes on which the source-only has al-

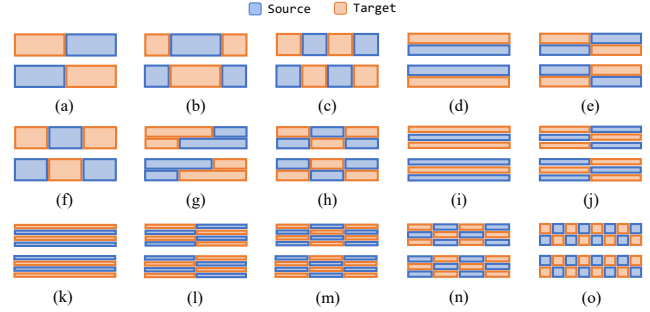


Figure 5. Different RV concatenation strategies.

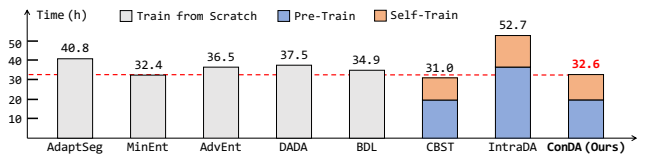


Figure 6. Training time (in hours) for each method.

ready performed well), ConDA yields considerable performance gains on almost all classes. This strongly supports our findings that fine-grained objects/background interactions in-between domains are conducive for the adaptations. **Qualitative Assessment.** Fig. 7 presents several visualization results for different lines of methods, *i.e.*, self-training (CBST [79]), adversarial training (DADA [61]), and both (IntraDA [41]). We observe that while the prior arts can only give limited improvements in certain areas, ConDA mitigates the false predictions holistically in most regions around the ego-vehicle. We accredit this to both the generalization ability provided by domain concatenation and the regularization enhancement offered by our anti-aliasing regularizer and entropy aggregator.

Training Complexity. Fig. 6 shows the training time of dif-

Method	barr	bicy	bus	car	const	moto	ped	cone	trail	truck	driv	othe	walk	terr	manm	veg	FloU	mIoU
Oracle	71.3	35.5	71.5	86.9	41.6	35.4	69.7	61.2	57.6	68.0	95.9	70.7	79.7	58.7	89.9	83.9	88.5	67.3
Source-only	15.5	7.9	20.6	70.5	16.1	3.6	41.9	11.4	0.5	40.6	90.2	10.7	41.7	19.1	77.4	74.5	73.4	33.9
AdaptSeg [57]	15.9	2.4	40.4	73.9	15.2	5.5	48.3	8.3	0.4	46.3	92.2	18.7	54.5	19.0	79.0	70.9	76.2	36.9
MinEnt [60]	19.2	0.2	36.1	73.2	15.7	6.2	50.3	10.8	0.8	45.0	91.5	24.1	54.8	21.7	78.7	71.8	76.0	37.5
AdvEnt [60]	12.5	9.0	43.0	74.1	14.7	7.0	51.4	12.7	0.5	47.0	91.4	14.5	53.6	19.2	80.1	73.4	76.2	37.8
DADA [61]	18.5	2.9	35.5	73.0	15.0	6.5	49.3	11.0	1.6	43.6	91.8	12.2	52.7	19.7	79.8	73.4	76.1	36.7
BDL _{PL} [30]	18.9	2.7	30.8	75.8	13.3	3.8	45.4	7.4	1.8	45.4	92.8	19.7	58.4	18.7	80.1	76.3	77.6	37.0
CBST [79]	17.7	1.4	33.6	75.0	13.3	6.4	52.3	12.3	1.9	46.9	92.5	22.8	57.2	19.7	80.2	77.3	77.5	38.1
AdaptSeg _{PL} [57]	10.5	0.6	33.5	71.3	17.2	5.2	41.9	11.4	1.0	43.5	90.4	18.5	60.1	20.0	80.0	74.6	76.1	36.3
IntraDA [41]	12.3	6.2	41.2	73.4	14.1	5.6	43.5	13.4	0.7	48.1	91.2	16.4	54.1	18.8	79.2	70.6	75.7	36.8
ConDA (Ours)	14.7	13.6	42.7	78.5	15.8	11.7	55.3	17.8	0.3	48.9	93.2	20.6	61.6	25.4	82.5	79.6	79.3	41.4

Table 5. Adaptation results for **Singapore** \rightarrow **Boston**. The methods are grouped, from top to bottom, as adversarial training, self-training, both, and ours. All IoU scores are given in percentage. Best score for each class is highlighted in **bold**.

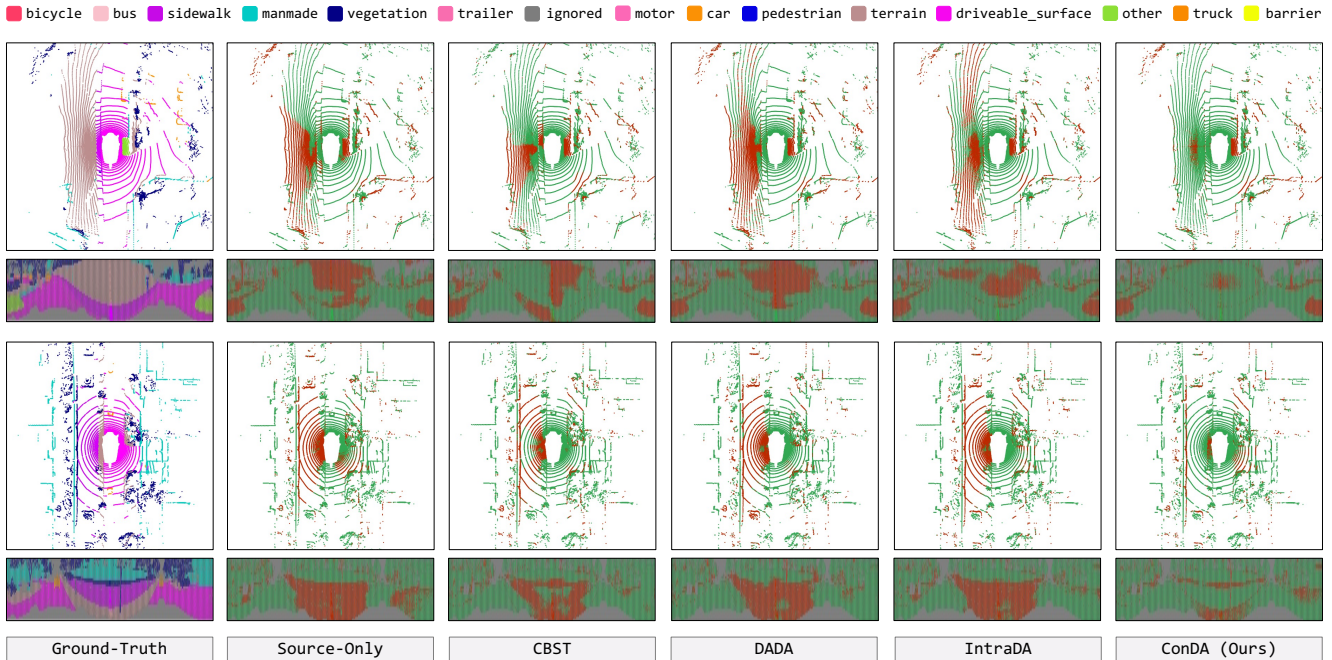


Figure 7. Qualitative results from both the bird’s eye view and range-view. To highlight the difference between the predictions and the ground-truth, the **correct** and **incorrect** points/pixels are painted in **green** and **red**, respectively. Best viewed in color.

ferent methods. Note that the pseudo-label generation time (around 1 hour) is excluded since this operation is usually conducted offline [25, 30, 79]. We find that while the inference speeds for these methods are similar (since they are sharing the same segmentation backbone), ConDA is still faster than most adversarial methods [57, 60, 61] which rely on additional discriminators for learning domain-invariant features during the adaptation. Our work is comparable with MinEnt [60] and CBST [79] in terms of speed but provides much better adaptation performance.

5. Conclusion

We presented ConDA, a concatenation-based domain adaptation framework that leverages the spatial coherency

in-between the source and target domains for fine-grained interactive learning. We also introduced an anti-aliasing regularizer and an entropy aggregator to reduce the detrimental effects of aliasing artifacts and noisy target predictions during pre-training and self-training. Extensive experiments on cross-city UDA scenarios showed that ConDA can bring overt segmentation performance improvements over baseline and competitive approaches. The robustness of our framework has shed light on flexible deployment in the perception modules of the autonomous driving system. In the future, we intend to dive deeper into the interactions between domains and will seek to extend our framework to other LiDAR domain adaptation scenarios, such as night/day, sunny/rainy, and synthetic/real adaptations.

Acknowledgements. We thank Sergi Widjaja, Xiaogang Wang, Edouard Francois Marc Capellier, and Dhananjai Sharma for insightful review and discussion.

References

- [1] Inigo Alonso, Luis Riazuelo Montesano, and Ana C. Murillo. Domain adaptation in lidar semantic segmentation. *arXiv preprint arXiv:2010.12239*, 2020. 3
- [2] Nikita Araslanov and Stefan Roth. Self-supervised augmentation consistency for adapting semantic segmentation. In *Proceedings of the IEEE/CVF Conference on Computer Vision and Pattern Recognition*, pages 15384–15394, 2021. 1
- [3] Jens Behley, Martin Garbade, Andres Milioto, Jan Quenzel, Sven Behnke, Cyrill Stachniss, and Jurgen Gall. Semantickitti: A dataset for semantic scene understanding of lidar sequences. In *Proceedings of the IEEE/CVF International Conference on Computer Vision*, pages 9297–9307, 2019. 1
- [4] David Berthelot, Nicholas Carlini, Ian Goodfellow, Nicolas Papernot, Avital Oliver, and Colin A. Raffel. Mixmatch: A holistic approach to semi-supervised learning. In *Advances in Neural Information Processing Systems*, 2019. 2, 3
- [5] Holger Caesar, Varun Bankiti, Alex H. Lang, Sourabh Vora, Venice Erin Liong, Qiang Xu, Anush Krishnan, Yu Pan, Giancarlo Baldan, and Oscar Beijbom. nuscenes: A multi-modal dataset for autonomous driving. In *Proceedings of the IEEE/CVF Conference on Computer Vision and Pattern Recognition*, pages 11621–11631, 2020. 1, 2, 3, 5
- [6] Yuan Cao, Zhiying Fang, Yue Wu, Ding-Xuan Zhou, and Quanquan Gu. Towards understanding the spectral bias of deep learning. *arXiv preprint arXiv:1912.01198*, 2019. 2, 5
- [7] Ming-Fang Chang, John Lambert, Patsorn Sangkloy, Jagjeet Singh, Slawomir Bak, Andrew Hartnett, De Wang, Peter Carr, Simon Lucey, Deva Ramanan, and James Hays. Argoverse: 3d tracking and forecasting with rich maps. In *Proceedings of the IEEE/CVF Conference on Computer Vision and Pattern Recognition*, pages 8748–8757, 2019. 1
- [8] Jaehoon Choi, Taekyung Kim, and Changick Kim. Self-ensembling with gan-based data augmentation for domain adaptation in semantic segmentation. In *Proceedings of the IEEE/CVF International Conference on Computer Vision*, pages 6830–6840, 2019. 3
- [9] Marius Cordts, Mohamed Omran, Sebastian Ramos, Timo Rehfeld, Markus Enzweiler, Rodrigo Benenson, Uwe Franke, Stefan Roth, and Bernt Schiele. The cityscapes dataset for semantic urban scene understanding. In *Proceedings of the IEEE/CVF Conference on Computer Vision and Pattern Recognition*, pages 3213–3223, 2016. 3
- [10] Dengxin Dai and Luc Van Gool. Dark model adaptation: Semantic image segmentation from daytime to nighttime. In *International Conference on Intelligent Transportation Systems*, pages 3819–3824, 2018. 3
- [11] Terrance DeVries and Graham W. Taylor. Improved regularization of convolutional neural networks with cutout. *arXiv preprint arXiv:1708.04552*, 2017. 2, 3, 7
- [12] Jiahua Dong, Yang Cong, Gan Sun, Yuyang Liu, and Xiaowei Xu. Cscl: Critical semantic-consistent learning for unsupervised domain adaptation. In *European Conference on Computer Vision*, pages 745–762, 2020. 3
- [13] Liang Du, Jingang Tan, Hongye Yang, Jianfeng Feng, Xiangyang Xue, Qibao Zheng, Xiaoqing Ye, and Xiaolin Zhang. Ssf-dan: Separated semantic feature based domain adaptation network for semantic segmentation. In *Proceedings of the IEEE/CVF International Conference on Computer Vision*, pages 982–991, 2019. 3
- [14] Whye Kit Fong, Rohit Mohan, Juana Valeria Hurtado, Lubing Zhou, Holger Caesar, Oscar Beijbom, and Abhinav Valada. Panoptic nuscenes: A large-scale benchmark for lidar panoptic segmentation and tracking. *arXiv preprint arXiv:2109.03805*, 2021. 1
- [15] Geoff French, Samuli Laine, Timo Aila, Michal Mackiewicz, and Graham Finlayson. Semi-supervised semantic segmentation needs strong, varied perturbations. *arXiv preprint arXiv:1906.01916*, 2019. 2
- [16] Yaroslav Ganin and Victor Lempitsky. Unsupervised domain adaptation by backpropagation. In *International Conference on Machine Learning*, pages 1180–1189, 2015. 1, 3
- [17] Yaroslav Ganin, Evgeniya Ustinova, Hana Ajakan, Pascal Germain, Hugo Larochelle, François Laviolette, Mario Marchand, and Victor Lempitsky. Domain-adversarial training of neural networks. *Journal of Machine Learning Research*, 17:1–35, 2016. 1, 3
- [18] Biao Gao, Yancheng Pan, Chengkun Li, Sibao Geng, and Huijing Zhao. Are we hungry for 3d lidar data for semantic segmentation? a survey of datasets and methods. *IEEE Transactions on Intelligent Transportation Systems*, 2021. 1
- [19] Jakob Geyer, Yohannes Kassahun, Mentar Mahmudi, Xavier Ricou, Rupesh Durgesh, Andrew S. Chung, Lorenz Hauswald, Viet Hoang Pham, Maximilian Mühlegg, Sebastian Dorn, Tiffany Fernandez, Martin Jänicke, Sudesh Mirashi, Chiragkumar Savani, Martin Sturm, Oleksandr Vorobiov, Martin Oelker, Sebastian Garreis, and Peter Schuberth. A2d2: Audi autonomous driving dataset. *arXiv preprint arXiv:2004.06320*, 2020. 1
- [20] Ian Goodfellow, Jean Pouget-Abadie, Mehdi Mirza, Bing Xu, David Warde-Farley, Sherjil Ozair, Aaron Courville, and Yoshua Bengio. Generative adversarial nets. In *Advances in Neural Information Processing Systems*, pages 2672–2680, 2014. 1, 3
- [21] Yves Grandvalet and Yoshua Bengio. Semi-supervised learning by entropy minimization. In *Proceedings of the International Conference on Neural Information Processing Systems*, pages 529–536, 2004. 2, 3
- [22] Kaiming He, Xiangyu Zhang, Shaoqing Ren, and Jian Sun. Deep residual learning for image recognition. In *Proceedings of the IEEE/CVF Conference on Computer Vision and Pattern Recognition*, pages 770–778, 2016. 3
- [23] Judy Hoffman, Eric Tzeng, Taesung Park, Jun-Yan Zhu, Phillip Isola, Kate Saenko, Alexei Efros, and Trevor Darrell. Cycada: Cycle-consistent adversarial domain adaptation. In *International Conference on Machine Learning*, pages 1989–1998, 2015. 3
- [24] John Houston, Guido Zuidhof, Luca Bergamini, Yawei Ye, Long Chen, Ashesh Jain, Sammy Omari, Vladimir

- Iglovikov, and Peter Ondruska. One thousand and one hours: Self-driving motion prediction dataset. *arXiv preprint arXiv:2006.14480*, 2020. 1
- [25] Maximilian Jaritz, Tuan-Hung Vu, Raoul de Charette, Emilie Wirbel, and Patrick Pérez. xmuda: Cross-modal unsupervised domain adaptation for 3d semantic segmentation. In *Proceedings of the IEEE/CVF Conference on Computer Vision and Pattern Recognition*, pages 12605–12614, 2020. 3, 5, 8
- [26] Peng Jiang and Srikanth Saripalli. Lidarnet: A boundary-aware domain adaptation model for point cloud semantic segmentation. In *IEEE International Conference on Robotics and Automation*, pages 2457–2464, 2021. 3
- [27] Myeongjin Kim and Hyeran Byun. Learning texture invariant representation for domain adaptation of semantic segmentation. In *Proceedings of the IEEE/CVF Conference on Computer Vision and Pattern Recognition*, pages 12975–12984, 2020. 3
- [28] Dong-Hyun Lee. Pseudo-label: The simple and efficient semi-supervised learning method for deep neural networks. In *International Conference on Machine Learning Workshop*, pages 896–901, 2013. 1, 3, 4
- [29] You Li and Javier Ibanez-Guzman. Lidar for autonomous driving: The principles, challenges, and trends for automotive lidar and perception systems. *IEEE Signal Processing Magazine*, 37(4):50–61, 2020. 1
- [30] Yunsheng Li, Lu Yuan, and Nuno Vasconcelos. Bidirectional learning for domain adaptation of semantic segmentation. In *Proceedings of the IEEE/CVF Conference on Computer Vision and Pattern Recognition*, pages 6936–6945, 2019. 3, 6, 7, 8
- [31] Jonathan Long, Evan Shelhamer, and Trevor Darrell. Fully convolutional networks for semantic segmentation. In *Proceedings of the IEEE/CVF Conference on Computer Vision and Pattern Recognition*, pages 3431–3440, 2015. 3
- [32] Ilya Loshchilov and Frank Hutter. Decoupled weight decay regularization. In *International Conference on Learning Representations*, 2018. 6
- [33] Yawei Luo, Liang Zheng, Tao Guan, Junqing Yu, and Yi Yang. Taking a closer look at domain shift: Category-level adversaries for semantics consistent domain adaptation. In *Proceedings of the IEEE/CVF Conference on Computer Vision and Pattern Recognition*, pages 2507–2516, 2019. 3
- [34] Yuce Luo, Jun Zhu, Mengxi Li, Yong Ren, and Bo Zhang. Smooth neighbors on teacher graphs for semi-supervised learning. In *Proceedings of the IEEE/CVF Conference on Computer Vision and Pattern Recognition*, pages 8896–8905, 2018. 2
- [35] Zhipeng Luo, Zhongang Cai, Changqing Zhou, Gongjie Zhang, Haiyu Zhao, Shuai Yi, Shijian Lu, Hongsheng Li, Shanghang Zhang, and Ziwei Liu. Unsupervised domain adaptive 3d detection with multi-level consistency. In *Proceedings of the IEEE/CVF International Conference on Computer Vision*, pages 8866–8875, 2021. 3
- [36] Haoyu Ma, Xiangru Lin, Zifeng Wu, and Yizhou Yu. Coarse-to-fine domain adaptive semantic segmentation with photometric alignment and category-center regularization. In *Proceedings of the IEEE/CVF Conference on Computer Vision and Pattern Recognition*, pages 4051–4060, 2021. 3
- [37] Ke Mei, Chuang Zhu, Jiaqi Zou, and Shanghang Zhang. Instance adaptive self-training for unsupervised domain adaptation. In *European Conference on Computer Vision*, pages 415–430, 2020. 3
- [38] Andres Milioto, Ignacio Vizzo, Jens Behley, and Cyrill Stachniss. Rangenet++: Fast and accurate lidar semantic segmentation. In *IEEE/RSJ International Conference on Intelligent Robots and Systems*, pages 4213–4220, 2019. 3
- [39] Gerhard Neuhold, Tobias Ollmann, Samuel Rota Buló, and Peter Kotschieder. The mapillary vistas dataset for semantic understanding of street scenes. In *Proceedings of the IEEE/CVF International Conference on Computer Vision*, pages 4990–4999, 2017. 3
- [40] Viktor Olsson, Wilhelm Trane, Juliano Pinto, and Lennart Svensson. Classmix: Segmentation-based data augmentation for semi-supervised learning. In *Proceedings of the IEEE/CVF Winter Conference on Applications of Computer Vision*, pages 1369–1378, 2021. 3
- [41] Fei Pan, Inkyu Shin, Francois Rameau, Seokju Lee, and In So Kweon. Unsupervised intra-domain adaptation for semantic segmentation through self-supervision. In *Proceedings of the IEEE/CVF Conference on Computer Vision and Pattern Recognition*, pages 3764–3773, 2020. 2, 3, 6, 7, 8
- [42] Sinno Jialin Pan and Qiang Yang. A survey on transfer learning. *IEEE Transactions on Knowledge and Data Engineering*, 22(10):1345–1359, 2009. 1
- [43] Duo Peng, Yinjie Lei, Wen Li, Pingping Zhang, and Yulan Guo. Sparse-to-dense feature matching: Intra and inter domain cross-modal learning in domain adaptation for 3d semantic segmentation. In *Proceedings of the IEEE/CVF International Conference on Computer Vision*, pages 7108–7117, 2021. 3
- [44] Alec Radford, Luke Metz, and Soumith Chintala. Unsupervised representation learning with deep convolutional generative adversarial networks. *arXiv preprint arXiv:1511.06434*, 2015. 3
- [45] Rindra Ramamonjison, Amin Banitalebi-Dehkordi, Xinyu Kang, Xiaolong Bai, and Yong Zhang. Simrod: A simple adaptation method for robust object detection. In *Proceedings of the IEEE/CVF International Conference on Computer Vision*, pages 3570–3579, 2021. 3, 7
- [46] Stephan R. Richter, Vibhav Vineet, Stefan Roth, and Vladlen Koltun. Playing for data: Ground truth from computer games. In *European Conference on Computer Vision*, pages 102–118, 2016. 3
- [47] German Ros, Laura Sellart, Joanna Materzynska, David Vazquez, and Antonio M. Lopez. The synthia dataset: A large collection of synthetic images for semantic segmentation of urban scenes. In *Proceedings of the IEEE/CVF Conference on Computer Vision and Pattern Recognition*, pages 3234–3243, 2016. 3
- [48] Aadarsh Sahoo, Rameswar Panda, Rogerio Feris, Kate Saenko, and Abir Das. Select, label, and mix: Learning discriminative invariant feature representations for partial domain adaptation. *arXiv preprint arXiv:2012.03358*, 2020. 3

- [49] Christos Sakaridis, Dengxin Dai, and Luc Van Gool. Accdc: The adverse conditions dataset with correspondences for semantic driving scene understanding. *arXiv preprint arXiv:2104.13395*, 2021. 3
- [50] Claude Elwood Shannon. A mathematical theory of communication. *the Bell System Technical Journal*, 27(3):379–423, 1948. 2
- [51] Samarth Sinha, Animesh Garg, and Hugo Larochelle. Curriculum by smoothing. *arXiv preprint arXiv:2003.01367*, 2020. 2, 5
- [52] Leslie N. Smith and Nicholay Topin. Super-convergence: Very fast training of neural networks using large learning rates. *arXiv preprint arXiv:1708.07120*, 2017. 6
- [53] Pei Sun, Henrik Kretzschmar, Xerxes Dotiwalla, Aurelien Chouard, Vijaysai Patnaik, Paul Tsui, James Guo, Yin Zhou Yuning Chai, Benjamin Caine, Vijay Vasudevan, Wei Han, Jiquan Ngiam, Hang Zhao, Aleksei Timofeev, Scott Ettinger, Maxim Krivokon, Amy Gao, Aditya Joshi, Yu Zhang, Jonathon Shlens, Zhifeng Chen, and Dragomir Anguelov. Scalability in perception for autonomous driving: Waymo open dataset. In *Proceedings of the IEEE/CVF Conference on Computer Vision and Pattern Recognition*, pages 2446–2454, 2020. 1
- [54] Marco Toldo, Andrea Maracani, Umberto Michieli, and Pietro Zanuttigh. Unsupervised domain adaptation in semantic segmentation: A review. *Technologies*, 8(2):1–35, 2020. 1
- [55] Wilhelm Tranheden, Viktor Olsson, Juliano Pinto, and Lennart Svensson. Dacs: Domain adaptation via cross-domain mixed sampling. In *Proceedings of the IEEE/CVF Winter Conference on Applications of Computer Vision*, pages 1379–1389, 2021. 3
- [56] Larissa T. Triess, Mariella Dreissig, Christoph B. Rist, and J. Marius Zöllner. A survey on deep domain adaptation for lidar perception. *arXiv preprint arXiv:2106.02377*, 2021. 3
- [57] Yi-Hsuan Tsai, Wei-Chih Hung, Samuel Schuster, Kihyuk Sohn, Ming-Hsuan Yang, and Manmohan Chandraker. Learning to adapt structured output space for semantic segmentation. In *Proceedings of the IEEE/CVF Conference on Computer Vision and Pattern Recognition*, pages 7472–7481, 2018. 3, 6, 7, 8
- [58] Cristina Vasconcelos, Hugo Larochelle, Vincent Dumoulin, Rob Romijnders, Nicolas Le Roux, and Ross Goroshin. Impact of aliasing on generalization in deep convolutional networks. In *Proceedings of the IEEE/CVF International Conference on Computer Vision*, pages 10529–10538, 2021. 2, 3, 5
- [59] Vikas Verma, Kenji Kawaguchi, Alex Lamb, Juho Kannala, Arno Solin, Yoshua Bengio, and David Lopez-Paz. Interpolation consistency training for semi-supervised learning. *Neural Networks*, 2021. 2, 3
- [60] Tuan-Hung Vu, Himalaya Jain, Maxime Bucher, Matthieu Cord, and Patrick Pérez. Advent: Adversarial entropy minimization for domain adaptation in semantic segmentation. In *Proceedings of the IEEE/CVF Conference on Computer Vision and Pattern Recognition*, pages 2517–2526, 2019. 2, 3, 6, 7, 8
- [61] Tuan-Hung Vu, Himalaya Jain, Maxime Bucher, Matthieu Cord, and Patrick Pérez. Dada: Depth-aware domain adaptation in semantic segmentation. In *Proceedings of the IEEE/CVF International Conference on Computer Vision*, pages 7364–7373, 2019. 3, 6, 7, 8
- [62] Haoran Wang, Tong Shen, Wei Zhang, Ling-Yu Duan, and Tao Mei. Classes matter: A fine-grained adversarial approach to cross-domain semantic segmentation. In *European Conference on Computer Vision*, pages 642–659, 2020. 3
- [63] Yuxi Wang, Junran Peng, and ZhaoXiang Zhang. Uncertainty-aware pseudo label refinery for domain adaptive semantic segmentation. In *Proceedings of the IEEE/CVF International Conference on Computer Vision*, pages 9092–9101, 2021. 2, 3, 5
- [64] Zhonghao Wang, Mo Yu, Yunchao Wei, Rogerio Feris, Jinjun Xiong, Wen mei Hwu, Thomas S. Huang, and Honghui Shi. Differential treatment for stuff and things: A simple unsupervised domain adaptation method for semantic segmentation. In *Proceedings of the IEEE/CVF Conference on Computer Vision and Pattern Recognition*, pages 12635–12644, 2020. 3
- [65] Garrett Wilson and Diane J. Cook. A survey of unsupervised deep domain adaptation. *ACM Transactions on Intelligent Systems and Technology*, 11(5):1–46, 2020. 1
- [66] Zuxuan Wu, Xintong Han, Yen-Liang Lin, Mustafa Gokhan Uzunbas, Tom Goldstein, Ser Nam Lim, and Larry S. Davis. Dcan: Dual channel-wise alignment networks for unsupervised scene adaptation. In *European Conference on Computer Vision*, pages 518–534, 2018. 3
- [67] Minghao Xu, Jian Zhang, Bingbing Ni, Teng Li, Chengjie Wang, Qi Tian, and Wenjun Zhang. Adversarial domain adaptation with domain mixup. In *Proceedings of the AAAI Conference on Artificial Intelligence*, pages 6502–6509, 2020. 3
- [68] Jinyu Yang, Weizhi An, Sheng Wang, Xinliang Zhu, Chaochao Yan, and Junzhou Huang. Label-driven reconstruction for domain adaptation in semantic segmentation. In *European Conference on Computer Vision*, pages 480–498, 2020. 3
- [69] Yanchao Yang and Stefano Soatto. Fda: Fourier domain adaptation for semantic segmentation. In *Proceedings of the IEEE/CVF Conference on Computer Vision and Pattern Recognition*, pages 4085–4095, 2020. 3
- [70] Fisher Yu, Haofeng Chen, Xin Wang, Wenqi Xian, Yingying Chen, Fangchen Liu, Vashisht Madhavan, and Trevor Darrell. Bdd100k: A diverse driving dataset for heterogeneous multitask learning. In *Proceedings of the IEEE/CVF Conference on Computer Vision and Pattern Recognition*, pages 2636–2645, 2020. 3
- [71] Xiangyu Yue, Bichen Wu, Sanjit A. Seshia, Kurt Keutzer, and Alberto L. Sangiovanni-Vincentelli. A lidar point cloud generator: From a virtual world to autonomous driving. In *ACM International Conference on Multimedia Retrieval*, pages 458–464, 2018. 1
- [72] Sangdoo Yun, Dongyoon Han, Seong Joon Oh, Sanghyuk Chun, Junsuk Choe, and Youngjoon Yoo. Cutmix: Regularization strategy to train strong classifiers with localizable fea-

- tures. In *Proceedings of the IEEE/CVF International Conference on Computer Vision*, pages 6023–6032, 2019. 2, 3, 7
- [73] Hongyi Zhang, Moustapha Cisse, Yann N. Dauphin, and David Lopez-Paz. mixup: Beyond empirical risk minimization. In *International Conference on Learning Representations*, 2018. 2, 3, 7
- [74] Richard Zhang. Making convolutional networks shift-invariant again. In *International Conference on Machine Learning*, pages 7324–7334, 2019. 2, 3, 5
- [75] Sicheng Zhao, Yezhen Wang, Bo Li, Bichen Wu, Yang Gao, Pengfei Xu, Trevor Darrell, and Kurt Keutze. epointda: An end-to-end simulation-to-real domain adaptation framework for lidar point cloud segmentation. *arXiv preprint arXiv:2009.03456*, 2020. 3
- [76] Zhedong Zheng and Yi Yang. Unsupervised scene adaptation with memory regularization in vivo. In *International Joint Conference on Artificial Intelligence*, pages 1076–1082, 2020. 2, 3
- [77] Barret Zoph, Golnaz Ghiasi, Tsung-Yi Lin, Yin Cui, Hanxiao Liu, Ekin D. Cubuk, and Quoc V. Le. Rethinking pre-training and self-training. In *Advances in Neural Information Processing Systems*, 2020. 1, 3
- [78] Xueyan Zou, Fanyi Xiao, Zhiding Yu, and Yong Jae Lee. Delving deeper into anti-aliasing in convnets. In *British Machine Vision Conference*, 2020. 2, 3, 5
- [79] Yang Zou, Zhiding Yu, B. V. K. Kumar, and Jinsong Wang. Unsupervised domain adaptation for semantic segmentation via class-balanced self-training. In *European Conference on Computer Vision*, pages 289–305, 2018. 1, 3, 4, 6, 7, 8
- [80] Yang Zou, Zhiding Yu, Xiaofeng Liu, B. V. K. Kumar, and Jinsong Wang. Confidence regularized self-training. In *Proceedings of the IEEE/CVF International Conference on Computer Vision*, pages 5982–5991, 2019. 3, 4